Odd-even $^{147-153}$Pm isotopes within the neutron-proton interacting boson-fermion model

J. Barea

Departamento de Física, Facultad de Ciencias Físicas y Matemáticas, Universidad de Concepción, Casilla 160-C, Concepción, Chile and Instituto de Estructura de la Materia, CSIC, Serrano 123, E-28006 Madrid, Spain

C. E. Alonso and J. M. Arias

Departamento de Física Atómica, Molecular y Nuclear, Facultad de Física, Universidad de Sevilla, Apartado 1065, 41080 Sevilla, Spain

(Received 2 November 2010; published 15 February 2011)

Low-lying energy states of the $^{147-153}$Pm isotopic chain are studied within the framework of the neutron-proton interacting boson-fermion model (IBFM-2). The spectra of these isotopes show a transition from a particle coupled to a vibrational core to a particle coupled to a deformed one. The calculation reproduces this behavior. In addition, reduced transition probabilities $B(E2)$ and $B(M1)$ and quadrupole and magnetic moments, as well as spectroscopic factors corresponding to stripping and pickup transfer reactions, are calculated. Obtained results compare well with the available experimental data, which reinforces the reliability of the wave functions obtained within the IBFM-2 model.

DOI: 10.1103/PhysRevC.83.024307 PACS number(s): 21.60.Fw, 21.10.Re, 21.10.Ky, 27.60.+j

I. INTRODUCTION

The improvement of the experimental techniques in the last years has made possible a considerable enlargement of the available experimental data on many nuclear species, among them, nuclei in the rare-earth region. In this region, the even-even nuclei within an isotopic chain show a transition from spherical vibrational shapes to well-deformed rotational ones. Similarly, in the odd-even nuclei a transition from particle-vibrator to particle-rotor is observed. The proper description of this transitional behavior is a challenge to any theoretical model. In this paper we concentrate on the comprehensive description of the nuclear structure of the odd-even $_{61}$Pm isotope chain. Their special features have recently made them to be the object of interest in theoretical studies as, for example, ^{151,153}Pm in Ref. [1]. In order to describe each nucleus and correlate the available data, the neutron-proton interacting boson-fermion model (IBFM-2) is used.

Since its introduction in the 1970s, the interacting boson model (IBM-1) has shown its ability to describe the collective low-lying spectra of medium mass and heavy even-even nuclei [2]. Soon after the introduction of the IBM-1, its extension to odd-even nuclei, called the interacting boson-fermion model (IBFM-1), was proposed [3,4]. The IBFM-1 has also shown to be successful in the description of low-lying collective states in odd-even nuclei in different nuclear regions [3]. Both IBM-1 and IBFM-1 do not distinguish between neutrons and protons. However, their extensions to include explicitly the neutron-proton degree of freedom were developed in parallel [2,3]. These extensions, usually called neutron-proton IBM (IBM-2) and neutron-proton IBFM (IBFM-2), provide a more direct connection with the shell model, giving a microscopic foundation to these models.

Odd-even promethium isotopes were studied in the mid-1980s [5] in the context of the IBFM-1 (without the explicit treatment of the neutron-proton degree of freedom). The results obtained accounted reasonably well for the available experimental data at that time. In order to include new experimental data [6,7], and to improve their description, the next natural step is to use the IBFM-2. This study can also shed light on shape transitions in odd-even systems, and it complements analogous calculations in this region of the nuclear chart [8]. Preliminary work in the description of the Pm isotopic chain was presented in Ref. [9].

The organization of the paper is the following. In Sec. II we briefly review the IBFM-2 model. The results, including energy spectra, $E2$ and $M1$ transition probabilities, quadrupole and magnetic moments, and spectroscopic factors for stripping and pickup reactions, are presented and discussed in Sec. III. The main conclusions are summarized in Sec. IV.

II. MODEL

The Hamiltonian used in the IBFM-2 includes pure boson and fermion terms and a boson-fermion interaction:

$$\hat{H} = \hat{H}_B + \hat{H}_F + \hat{V}_{BF}, \tag{1}$$

where

$$\hat{H}_B = \varepsilon(\hat{n}_{d_\nu} + \hat{n}_{d_\pi}) + \kappa\,\hat{Q}_\nu \cdot \hat{Q}_\pi + \hat{V}_{\pi\pi} + \hat{V}_{\nu\nu} + \xi\,\hat{M}_{\pi\nu}, \tag{2}$$

$$\hat{H}_F = \sum_j \epsilon_j a_j^\dagger \cdot \tilde{a}_j, \tag{3}$$

and

$$\hat{V}_{BF} = \Gamma_\pi \hat{V}^Q_{\nu\pi} - \Lambda_\pi \hat{V}^E_{\nu\pi} + A_\pi \hat{V}^M_{\nu\pi}. \tag{4}$$

In the following, the treatment for an odd-proton nucleus is assumed.

The operators appearing in $\hat{H}_B$ are $\hat{n}_{d_\rho}$, the number of d bosons of kind ρ ($\rho = \nu, \pi$ for neutrons and protons,

respectively),

$$\hat{Q}_\rho = [s^\dagger \times \tilde{d} + d^\dagger \times \tilde{s}]^{(2)}_\rho + \chi_\rho [d^\dagger \times \tilde{d}]^{(2)}_\rho, \quad (5)$$

$$\hat{V}_{\rho\rho} = \sum_{L=0,2,4} \frac{C_L^{(\rho)}}{2} [d^\dagger_\rho \times d^\dagger_\rho]^{(L)} \cdot [\tilde{d}_\rho \times \tilde{d}_\rho]^{(L)}, \quad (6)$$

$$\hat{M}_{\pi\nu} = \frac{1}{2}[s^\dagger_\nu \times d^\dagger_\pi - s^\dagger_\pi \times d^\dagger_\nu]^{(2)} \cdot [\tilde{s}_\nu \times \tilde{d}_\pi - \tilde{s}_\pi \times \tilde{d}_\nu]^{(2)} - \sum_{k=1,3} [d^\dagger_\nu \times d^\dagger_\pi]^{(k)} \cdot [\tilde{d}_\nu \times \tilde{d}_\pi]^{(k)}, \quad (7)$$

where $s^\dagger_\rho$ and $d^\dagger_\rho$ are boson creation operators with $L = 0$ and $L = 2$, respectively, while $a^\dagger_{jm}$ is the odd-proton creation operator in the $|nl\frac{1}{2}jm\rangle$ single particle level, where, for convenience, we omit the labels $nl\frac{1}{2}$. $\tilde{s}$, $\tilde{d}$, and $\tilde{a}$ are annihilation operators, with the proper tensorial behavior under rotations, defined as $\tilde{s} = s$, $\tilde{d}_\mu = (-1)^\mu d_{-\mu}$, and $\tilde{a}_{jm} = (-1)^{j-m} a_{j-m}$. The terms appearing in the boson-fermion interaction (4) read

$$\hat{V}^Q_{\nu\pi} = \sum_{jj'} \langle l, 1/2;\ j||Y^{(2)}||l', 1/2;\ j'\rangle \times (u_j u_{j'} - v_j v_{j'}) \hat{Q}_\nu \cdot [a^\dagger_j \times \tilde{a}_{j'}]^{(2)}_\pi, \quad (8)$$

$$\hat{V}^E_{\nu\pi} = \sum_{jj'j''} \sqrt{\frac{10}{(2j+1)N_\pi}} \frac{\beta_{jj'}\beta_{j''j}}{K^2_\beta} \times \{\hat{Q}_\nu \cdot [(d^\dagger \times \tilde{a}_{j''})^{(j)} \times (\tilde{s} \times a^\dagger_{j'})^{(j')}]^{(2)}_\pi + \text{h.c.}\}, \quad (9)$$

$$\hat{V}^M_{\nu\pi} = \hat{n}_{d_\nu} \cdot \hat{n}_\pi \quad (10)$$

where N_ρ is the number of ρ bosons, and

$$\beta_{jj'} = (u_j v_{j'} + v_j u_{j'}) \times \langle l, 1/2; j||Y^{(2)}||l', 1/2; j'\rangle, \quad (11)$$

$$K_\beta = \sqrt{\sum_{jj'} \beta^2_{jj'}}. \quad (12)$$

The quasiparticle energies ϵ_j [Eq. (3)] and the occupation probabilities v_j [Eqs. (8)–(11)] are obtained from a BCS calculation using the following set of coupled equations:

$$\epsilon_j = \sqrt{\left(E^{\text{sp}}_j - \lambda\right)^2 + \Delta^2}, \quad (13)$$

$$v^2_j = \frac{1}{2}\left(1 - \frac{E^{\text{sp}}_j - \lambda}{\epsilon_j}\right). \quad (14)$$

E^{sp}_j are the energies of the single-particle levels which the odd proton can occupy, $\Delta = 12A^{-1/2}$ (MeV) is the pairing gap, and λ is the Fermi level obtained from this calculation, which is constrained to the conservation of the number of particles

$$2N_\pi = \sum_j v^2_j (2j+1). \quad (15)$$

III. DESCRIPTION OF THE ODD-EVEN Pm ISOTOPES

An odd-even $_{61}$Pm isotope is described in IBFM-2 by coupling a proton to its $_{60}$Nd isotone, described in terms of the IBM-2, with the Hamiltonian of Eq. (2). Consequently, the first step to describe the odd-even nucleus is a compelling description of the even-even core. In the case of the Pm isotopes, Ref. [10] was taken as a starting point for the description of the Nd even-even cores. Afterward, the parameters were slightly changed to take into account later experimental information on mixed symmetry states 1^+ [11]. The resulting values of the parameters used in the description of the Nd cores can be found in Table I. The strength of the Majorana interaction, $\hat{M}_{\pi\nu}$, was obtained by fitting the excitation energy of the first 1^+ level, mixed symmetry state allowed in IBM-2, but not in IBM-1. With those parameters, both energy spectra and electromagnetic properties were calculated in good agreement with the available experimental data for even-even Nd isotopes. Thus, we are confident that the wave functions of the even-even Nd core nuclei provided by the IBM-2 model are good.

TABLE I. Parameters different from zero (ϵ, κ, and ξ in MeV) used in Eq. (2) for the description of the even-even Nd isotopes ($N_\pi = 5$). The values $\chi_\pi = -1.2$, $C_0^{(\pi)} = 0.4$ MeV, and $C_2^{(\pi)} = 0.2$ MeV are fixed for all the isotopes.

A	146	148	150	152
N_ν	2	3	4	5
ε	0.90	0.70	0.47	0.34
κ	−0.15	−0.10	−0.07	−0.089
χ_ν	0.00	−0.80	−1.00	−1.10
ξ	0.08	0.22	0.37	0.22

Once the wave functions for the states in the even-even core have been obtained, the odd-proton has to be coupled to it in order to calculate excitation energies, electromagnetic properties, and spectroscopic strengths in the odd-even Pm isotopes.

A. Excitation energies

The coupling of the proton to the even-even core is governed by the boson-fermion interaction, where the more important terms are those between the odd fermion (proton for Pm isotopes) and the bosons with the alternative flavor (neutrons in our case). This interaction, Eq. (4), is decomposed into three terms: quadrupole ($\hat{V}^Q_{\nu\pi}$), exchange ($\hat{V}^E_{\nu\pi}$), and monopole ($\hat{V}^M_{\nu\pi}$). Since the Hamiltonian is invariant under parity, positive and negative parity states are studied separately. The parameters in $\hat{V}_{BF}$ are different for each parity accordingly and are shown in Table II. It is important to emphasize that Γ_π, Λ_π, and A_π are phenomenological parameters for the entire chain of isotopes, in contrast to the above-mentioned IBFM-1 calculation, where these parameters were fitted for each isotope separately.

TABLE II. Parameters (in MeV) of the boson-fermion interaction (4) used in this work for positive (+) and negative (−) parity states.

Parity	Γ_π	Λ_π	A_π
+	0.452	0.030	−0.097
−	0.883	4.885	−0.866

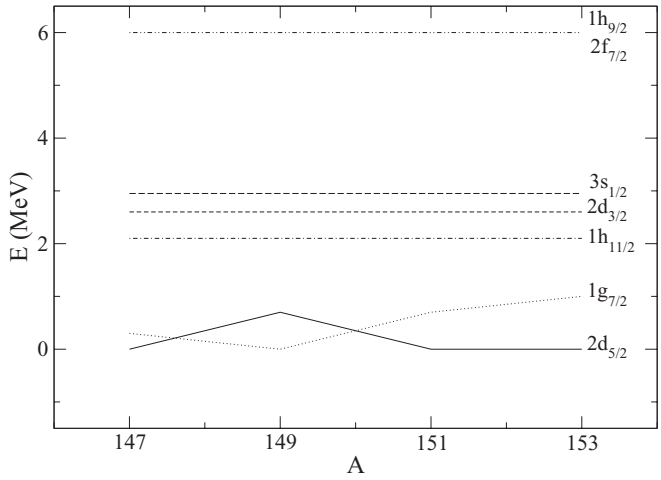

FIG. 1. Single-particle energies used in the BCS calculation for each isotope.

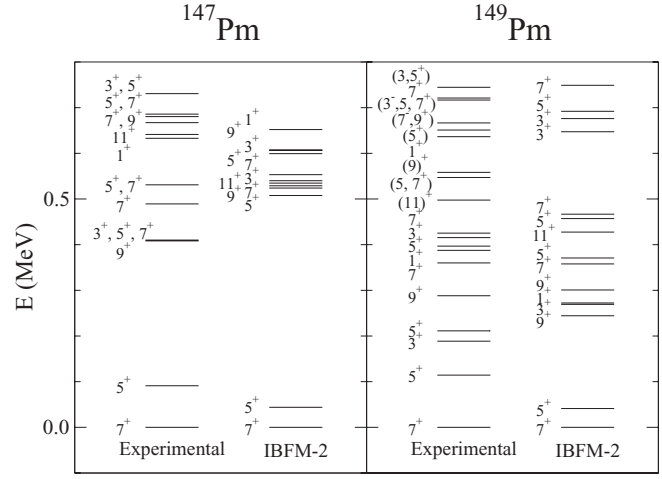

FIG. 2. Measured and calculated excitation energies (in MeV) of the positive parity levels in ^{147}Pm and ^{149}Pm. Experimental data have been taken from Refs. [16,17]. The numbers indicate twice the angular momentum.

The single-particle energies $E_j^{\rm sp}$ appearing in Eqs. (13) and (14) are plotted in Fig. 1. These were taken from Ref. [12], but we changed the relative position of the $1g_{7/2}$ and $2d_{5/2}$ orbits to account for the sequence in the low-lying levels $J^\pi = \frac{5}{2}^+$ and $J^\pi = \frac{7}{2}^+$ along the chain of isotopes. This variation of the positions of $1g_{7/2}$ and $2d_{5/2}$ (especially for ^{149}Pm) somehow disturbs the impression that the whole chain is described in a consistent way. However, the same problem has been encountered in calculations for other nuclei close to the ones considered in this work [8,13–15]. The origin of this anomaly is not clear and requires a specific study. Table III shows the quasiparticle energies and the occupation probabilities obtained from the BCS calculation. One important feature to note is that the positive parity levels $2d_{3/2}$ and $3s_{1/2}$ as well as the negative parity levels $1h_{9/2}$ and $2f_{7/2}$ have high quasiparticle energies and small occupation probabilities when we compare them with the rest of the levels of the same parity. This allows us to consider only the levels $2d_{5/2}$ and $1g_{7/2}$ for positive parity and $1h_{11/2}$ for negative parity, as was done in Ref. [5].

In Fig. 2, experimental and calculated excitation energies of the positive parity levels in ^{147}Pm and ^{149}Pm are shown. The correspondence between experimental and calculated levels was done using the electromagnetic properties discussed below. It can be seen that the structure of the spectrum of ^{147}Pm corresponds to a particle coupled to a vibrational core. The first two states come from the coupling of the single-particle states included in the calculation with the ground state of ^{146}Nd. Then there is a gap and, around the energy of the first 2^+ of ^{146}Nd (453.77 keV), a set of levels, which comes from the coupling of the single-particle levels to this state, appears. The spectrum of ^{149}Pm corresponds to a transitional situation where the forbidden zone (gap) is absent. Our calculations reproduce well this structure, although they show a certain tendency to structures of the particle-vibration type in both isotopes. The origin of this effect can be found in the low values of the boson-fermion parameters, which supply weak coupling schemes.

Experimental and calculated excitation energies of the negative parity levels in ^{147}Pm and ^{149}Pm are compared in Fig. 3. The correspondence in this case is difficult for some levels in ^{147}Pm, due to the lack of electromagnetic information which would allow for their correct identification. Nevertheless, from the excitation energies, it seems that the $\frac{5}{2}^-$, $\frac{7}{2}^-$ level at 0.158 MeV above the lowest negative parity state is missing in our calculation. This fact was also

TABLE III. Quasiparticle energies (in MeV) and occupation probabilities squared obtained from a BCS calculation for the odd-proton Pm isotopes using the single-particle energies plotted in Fig. 1.

A	146		148		150		152	
	ϵ_j	v^2	ϵ_j	v^2	ϵ_j	v^2	ϵ_j	v^2
$2d_{\frac{5}{2}}$	1.0852	0.7016	0.9947	0.4355	1.1817	0.7795	1.2801	0.8247
$1g_{\frac{7}{2}}$	1.0026	0.5686	1.1401	0.7507	0.9806	0.4799	0.9878	0.4147
$1h_{\frac{11}{2}}$	1.9365	0.0708	1.8190	0.0799	1.7412	0.0867	1.5990	0.1033
$2d_{\frac{3}{2}}$	2.3796	0.0456	2.2555	0.0503	2.1728	0.0537	2.0187	0.0620
$3s_{\frac{1}{2}}$	2.7016	0.0350	2.5748	0.0381	2.4902	0.0403	2.3315	0.0457
$1h_{\frac{9}{2}}, 2f_{\frac{7}{2}}$	5.6504	0.0078	5.5172	0.0081	5.4285	0.0082	5.2595	0.0086

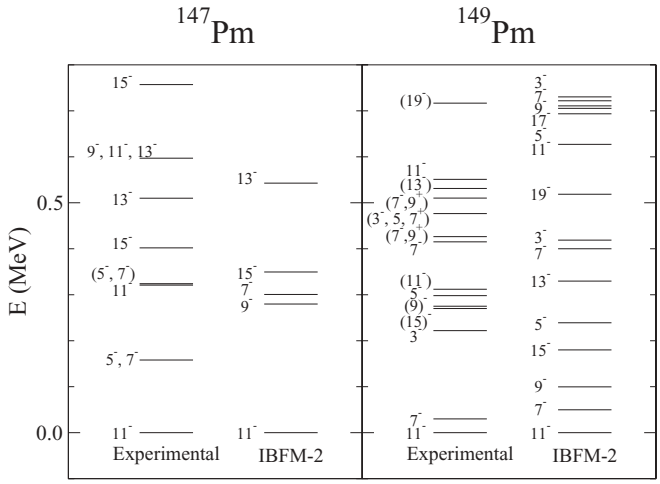

FIG. 3. Same as Fig. 2, but for the negative parity levels in ^{147}Pm and ^{149}Pm. Experimental data have been taken from Refs. [16,17].

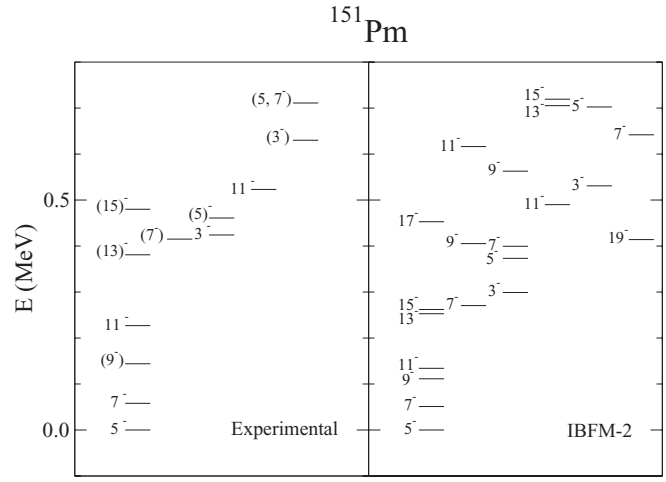

FIG. 5. Same as Fig. 2, but for the negative parity levels in ^{151}Pm. Experimental data have been taken from Ref. [18].

observed in the IBFM-1 calculation [5], where it was suggested that this level could be reproduced when the 3^-_1 level of ^{146}Nd is included, which is beyond the scope of this work. The calculation for the ^{149}Pm isotope shows a sequence of levels distributed almost uniformly up to 0.7 MeV, while there is a set of experimental levels grouped together around 0.3 MeV. However, there is an almost 1:1 correspondence between experimental and calculated levels below 0.5 MeV.

The structure of the energy spectra for the ^{151}Pm and ^{153}Pm nuclei look different when compared to the above-discussed isotopes and corresponds to a particle coupled to a rotational core. The experimental and calculated levels are organized in bands according to the $B(E2)$ values in Figs. 4 and 5 for positive and negative parity states of ^{151}Pm, respectively, and in Figs. 6 and 7 for positive and negative parity states of ^{153}Pm, respectively. The overall agreement between the calculation and the experimental data is good.

It can be seen in Fig. 4 that, in ^{151}Pm, the ground state and the second calculated excited bands are fairly well reproduced. Moreover, our calculations indicate the existence of a first excited band led by a $7/2^+$ state at approximately 0.25 MeV, followed by a $9/2^+$ state at 0.4 MeV. Regarding the negative parity levels, those of the lowest band are reproduced in the right order, showing departures, specially in those with high angular momentum. However the bandhead angular momenta are correctly reproduced by the calculation.

Finally, as it can be seen in Fig. 6 that in ^{153}Pm there is an excellent agreement between the calculated and the experimental energies for the positive parity levels. Again, the calculation predicts a first excited band led by a $7/2^+$ state at around 0.4 MeV. In the case of the negative parity levels, Fig. 7, experimental data are only available for the ground-state band, well described in the calculation, but with a slightly higher moment of inertia. A first excited band, led by a $7/2^-$ state at 0.2 MeV, appears in our calculations, as in ^{151}Pm.

Figures 8 and 9 show experimental and calculated energies of the low-lying energy levels in odd-even Pm isotopes versus the mass number for positive and negative parity, respectively. The goal of these figures is to show the systematics of the levels. We can observe two different trends for the positive

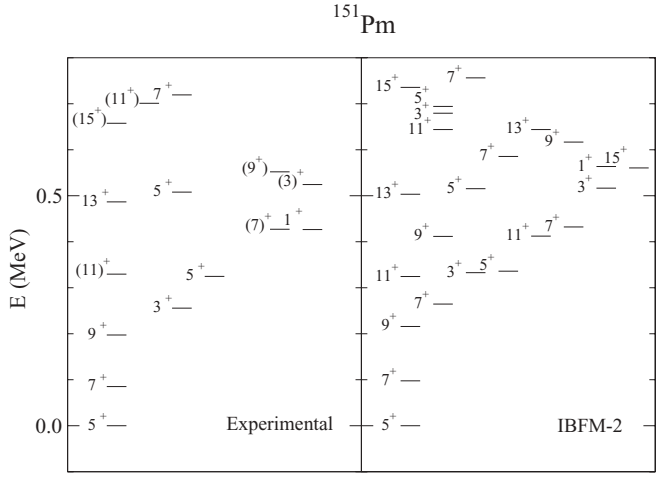

FIG. 4. Same as Fig. 2, but for the positive parity levels in ^{151}Pm. Experimental data have been taken from Ref. [18].

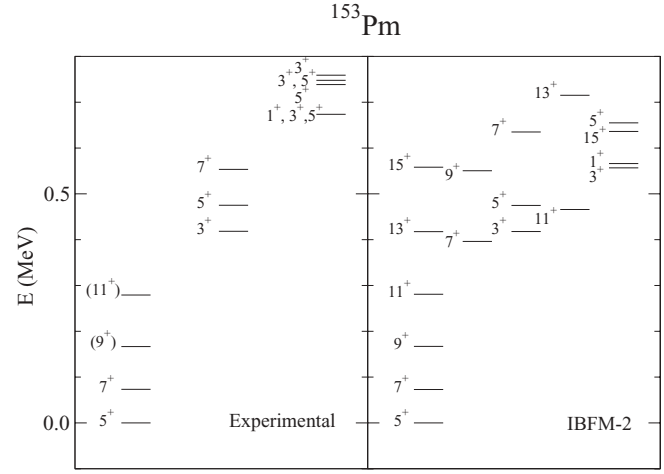

FIG. 6. Same as Fig. 2, but for the positive parity levels in ^{153}Pm. Experimental data have been taken from Ref. [19].

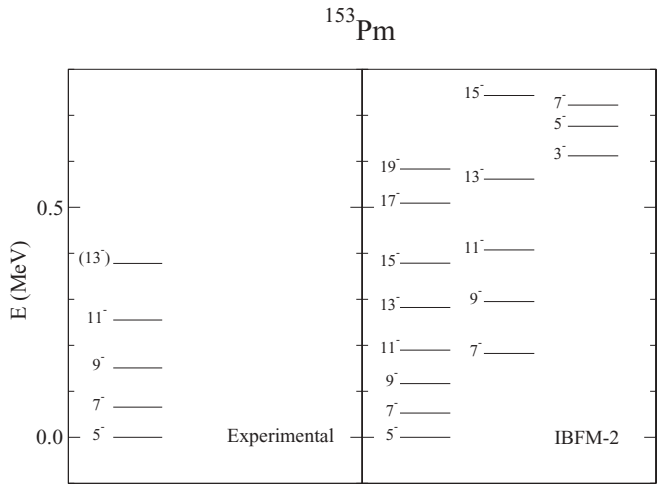

FIG. 7. Same as Fig. 2, but for the negative parity levels in ^{153}Pm. Experimental data have been taken from Ref. [19].

parity levels, there are some levels that present a monotonous decrease in energy while for others a minimum develops in an intermediate isotope. The calculation is able to reproduce these behaviors. Negative parity levels show a decreasing behavior which is well described in the calculations.

To finalize this subsection, we can assert that IBFM-2 reproduces well the complicated structure of the energy levels, although deviations with regard to the experimental data are observed when studying a particular nucleus. A detailed study of a certain isotope is feasible, but it would involve a fine tuning of the Hamiltonian parameters, which is not the aim of this work.

B. Electromagnetic properties

In addition to spectra, we have calculated $B(E2)$'s and $B(M1)$'s to compare them with their experimental values. This

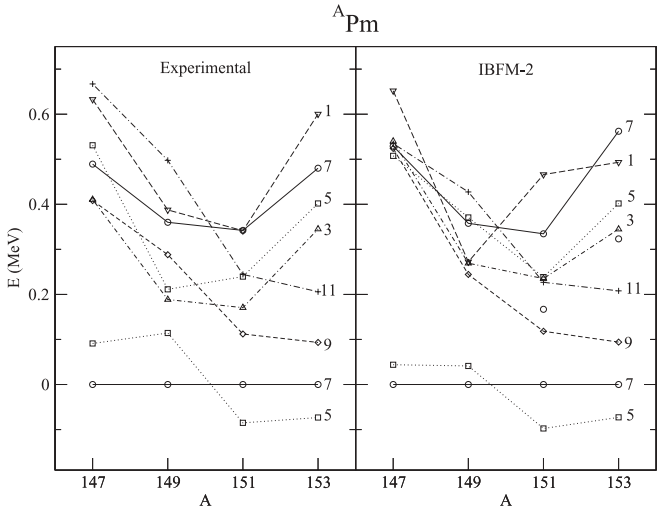

FIG. 8. Experimental and calculated excitation energies for the low-lying positive parity states of odd-even Pm isotopes. The energy of the first $\frac{7}{2}^+$ is taken as reference.

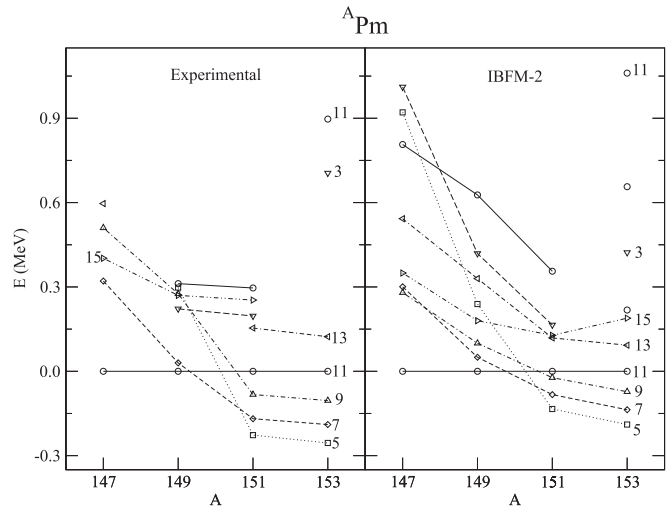

FIG. 9. Experimental and calculated energies for the low-lying negative parity states of odd-even Pm isotopes. The energy of the first $\frac{11}{2}^-$ is taken as a reference.

comparison allows us to establish the degree of reliability of the wave functions obtained in this work.

The electric quadrupole transition operator $\hat{T}^{(E2)}$ consists of a bosonic and a fermionic part:

$$\hat{T}^{(E2)} = \hat{T}^{(E2)}_B + \hat{T}^{(E2)}_F, \tag{16}$$

where

$$\hat{T}^{(E2)}_B = e_\pi \hat{Q}_\pi + e_\nu \hat{Q}_\nu, \tag{17}$$

$$\hat{T}^{(E2)}_F = -\frac{e_F}{\sqrt{5}} \sum_{j \leqslant j'} (u_j u_{j'} - v_j v_{j'}) \left\langle l \tfrac{1}{2} j \left\| r^2 Y^{(2)} \right\| l' \tfrac{1}{2} j' \right\rangle \times ([a^\dagger_j \times \tilde{a}_{j'}]^{(2)} + \text{h.c.}). \tag{18}$$

The quadrupole operators present in $\hat{T}^{(E2)}_B$ correspond to those appearing in the Hamiltonian (5). The value used for the bosonic effective charges e_π and e_ν is 0.139 e b, taken from Ref. [5]. For the fermionic effective charge e_F, we adopt the value 1.5 e b. As usual in the literature, we take constant values for the radial part in the reduced matrix element of $r^2 Y^{(2)}$. Analogously, the magnetic dipole transition operator $\hat{T}^{(M1)}$ is made up of a bosonic and a fermionic part,

$$\hat{T}^{(M1)} = \hat{T}^{(M1)}_B + \hat{T}^{(M1)}_F, \tag{19}$$

where

$$\hat{T}^{(M1)}_B = \sqrt{\frac{3}{4\pi}} (g_\pi \hat{L}_\pi + g_\nu \hat{L}_\nu), \tag{20}$$

$$\hat{T}^{(M1)}_F = -\sqrt{\frac{1}{4\pi}} \sum_{j \leqslant j'} (u_j u_{j'} + v_j v_{j'}) \left\langle l \tfrac{1}{2} j \left\| g_l \vec{l} + g_s \vec{s} \right\| l' \tfrac{1}{2} j' \right\rangle \times ([a^\dagger_j \times \tilde{a}_{j'}]^{(1)} + \text{h.c}), \tag{21}$$

with $\hat{L}_\rho = \sqrt{10}(d^\dagger_\rho \times \tilde{d}_\rho)^{(1)}$. The bosonic gyromagnetic factors g_π and g_ν have been extracted from Ref. [20] and their values are shown in Table IV.

TABLE IV. Bosonic gyromagnetic factors (in μ_N) used in this work (extracted from Ref. [20]).

A	147	149	151	153
g_ν	−0.183	−0.171	−0.159	−0.147
g_π	0.415	0.415	0.415	0.415

The adopted values for the orbital and spin fermionic gyromagnetic factors are $g_l = 1.0\ \mu_N$ and $g_s = 4.0\ \mu_N$ (the spin gyromagnetic factor was quenched 70% with respect to the value of the free proton, as usually found in the literature).

Figure 10 shows the trend of the calculated values of $B(E2)$ for some low-lying positive parity states in the Pm isotopes along with their experimental counterparts. The calculation reproduces well the trend, except the transition $3/2_1^+ \to 7/2_1^+$ for $A = 147$. These could be due to the existence of a low energy state 0^+ at 915.4 keV in the even-even core, ^{146}Nd, which the IBM is unable to reproduce without including octupole degrees of freedom [21]. The coupling of this state with the fermionic single-particle degrees of freedom may have a relatively high influence on the low-lying states in ^{147}Pm. Table V shows additional experimental and calculated values of $B(E2)$ and $B(M1)$ for this nucleus. It can be seen that, even when the calculation does not describe fine details of the experimental data, general trends are reproduced. Again the inclusion of octupole degrees of freedom could improve the description of this nucleus. Some calculated and experimental values of the reduced transition probabilities $B(E2)$ and $B(M1)$ in ^{149}Pm are quoted in Table VI. The agreement between the calculation and the experimental data is reasonable. Notice that the calculated values of $B(E2)$ and $B(M1)$ for the transition from $5/2_2^+$ to $7/2_1^+$ are lower than the corresponding ones from $5/2_3^+$ which is closer to the experimental situation. This allows us to identify the calculated state $5/2_3^+(5/2_2^+)$ with the experimental state $5/2_2^+(5/2_3^+)$. This kind of exchange was observed in the previous IBFM-1 calculation, but between the states $5/2_1^+$ and $5/2_2^+$. The same

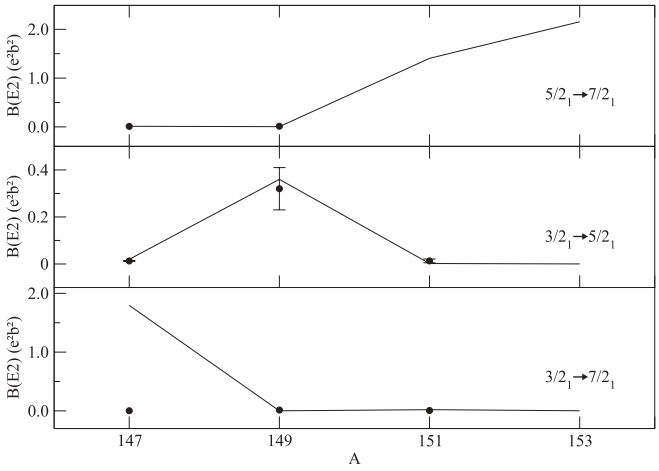

FIG. 10. Experimental (symbols) [16–19] and calculated (lines) electric quadrupole reduced transition probabilities between some low-lying states in ^{A}Pm.

TABLE V. Experimental [16] and calculated electric quadrupole (in e^2 b^2) and magnetic dipole (in μ_N^2) reduced transition probabilities between some low-lying states of ^{147}Pm.

$J_i^\pi \to J_f^\pi$			$J_i^\pi \to J_f^\pi$		
$B(E2)$	Expt.	IBFM-2	$B(M1)$	Expt.	IBFM-2
$\frac{5}{2}^+_2 \to \frac{3}{2}^+_1$	0.0018(18)	0.0141	$\frac{5}{2}^+_1 \to \frac{7}{2}^+_1$	0.0067(2)	0.0001
$\frac{5}{2}^+_2 \to \frac{5}{2}^+_1$	0.0009(4)	0.0020	$\frac{3}{2}^+_1 \to \frac{5}{2}^+_1$	0.0068(9)	0.0127
$\frac{5}{2}^+_2 \to \frac{7}{2}^+_1$	0.0019(5)	0.2075	$\frac{5}{2}^+_2 \to \frac{3}{2}^+_1$	0.007(3)	0.023
$\frac{5}{2}^+_3 \to \frac{7}{2}^+_2$	0.0023(23)	0.0000	$\frac{5}{2}^+_2 \to \frac{5}{2}^+_1$	0.0003(1)	0.0063
$\frac{5}{2}^+_3 \to \frac{3}{2}^+_1$	0.0010(5)	0.0146	$\frac{5}{2}^+_2 \to \frac{7}{2}^+_1$	0.0023(5)	0.0009
$\frac{5}{2}^+_3 \to \frac{7}{2}^+_1$	0.0003(1)	0.0015	$\frac{5}{2}^+_3 \to \frac{7}{2}^+_2$	0.0016(9)	0.0090
			$\frac{5}{2}^+_3 \to \frac{5}{2}^+_1$	0.0027(11)	0.0202
			$\frac{5}{2}^+_3 \to \frac{7}{2}^+_1$	0.0001(1)	0.0021

happens with the calculated states $1/2_{1,2}^+$, which we have identified with the experimental states $1/2_{2,1}^+$. Experimental data on electromagnetic transitions are scarce for the nucleus ^{151}Pm and absent, to the best of our knowledge, for the nucleus ^{153}Pm. Figure 11 shows the trend of the electric quadrupole moments of the $5/2_1^+$ and $7/2_1^+$ states and of the magnetic dipole moments of the $3/2_1^+$, $5/2_1^+$, and $7/2_1^+$ states. Experimental electric quadrupole moments are nicely reproduced by the calculation, in contrast to magnetic dipole moments, whose description is clearly worse. Nevertheless we can conclude that the description of the electromagnetic properties with IBFM-2 is equal to or slightly better than the one obtained with IBFM-1.

C. Spectroscopic factors

Another important tool for checking the quality of the description of odd-even nuclei is provided by one-nucleon transfer reactions. For this reason we will analyze spectroscopic factors of one-proton stripping and pickup reactions having as final nuclei the Pm isotopes we are studying.

TABLE VI. Experimental [17] and calculated electric quadrupole (in e^2 b^2) and magnetic dipole (in μ_N^2) reduced transition probabilities between some low-lying states of ^{149}Pm.

$J_i^\pi \to J_f^\pi$			$J_i^\pi \to J_f^\pi$		
$B(E2)$	Expt.	IBFM-2	$B(M1)$	Expt.	IBFM-2
$\frac{5}{2}^+_2 \to \frac{7}{2}^+_1$	0.18(4)	0.06	$\frac{5}{2}^+_1 \to \frac{7}{2}^+_1$	0.0049(1)	0.0009
$\frac{1}{2}^+_1 \to \frac{5}{2}^+_2$	0.014(4)	0.036	$\frac{3}{2}^+_1 \to \frac{5}{2}^+_1$	0.0025(7)	0.0686
$\frac{1}{2}^+_1 \to \frac{5}{2}^+_1$	0.006(2)	0.000	$\frac{5}{2}^+_2 \to \frac{7}{2}^+_1$	0.034(7)	0.047
$\frac{7}{2}^-_1 \to \frac{11}{2}^-_1$	0.61(19)	0.60	$\frac{5}{2}^+_2 \to \frac{5}{2}^+_1$	0.022(5)	0.012
$\frac{5}{2}^+_3 \to \frac{7}{2}^+_1$	–	0.008	$\frac{5}{2}^+_2 \to \frac{3}{2}^+_1$	0.007(3)	0.023
			$\frac{1}{2}^+_1 \to \frac{3}{2}^+_1$	0.0057(13)	0.0003

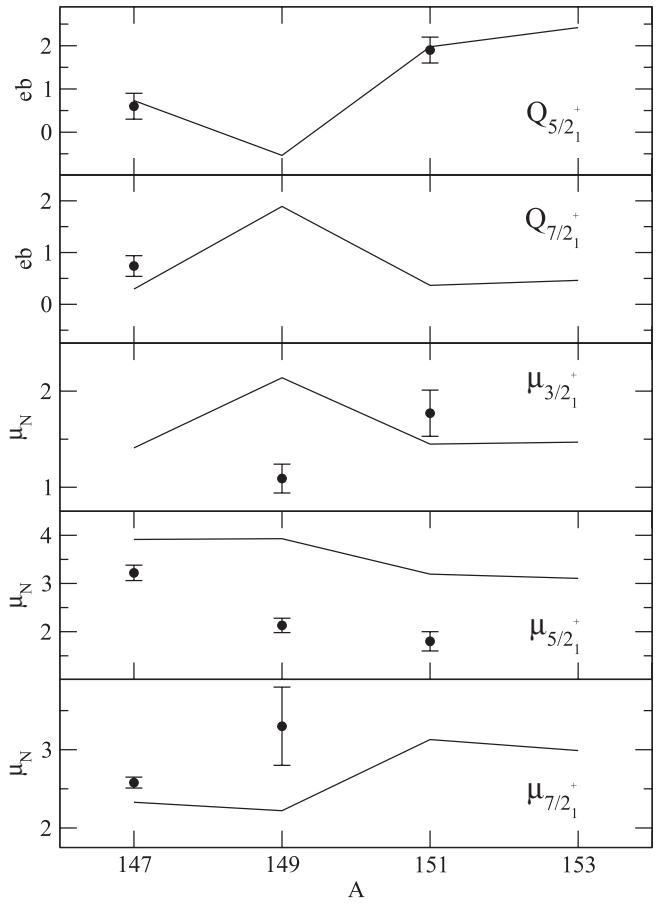

FIG. 11. Experimental (symbols) [16–19] and calculated (lines) electric quadrupole and magnetic dipole moments of some low-lying states in ^{A}Pm.

The image of the one-fermion transfer operator in the boson-fermion space of the IBFM-2 is an expansion that can be obtained using different techniques and approximations.

The first order (FO) operator for a boson-conserving reaction is

$$(\hat{T}_{jm})_{\rm FO} = u_j a^\dagger_{jm}. \tag{22}$$

A more elaborate possibility is to use the boson image of the shell model particle creation operator obtained using the Otsuka-Arima-Iachello (OAI) method [22], where states with Generalized Seniority (GS) as a good quantum number are used. This turns out to be valid for nuclei close to closed shells, and its expression is

$$\begin{aligned}(\hat{T}_{jm})_{\rm GS} = {} & u_j a^\dagger_{jm} + \frac{v_j}{\sqrt{N_\pi}}[s^\dagger_\pi \times \tilde{a}_j]^{(j)}_m \\ & + \sum_{j'} u_j \sqrt{\frac{10}{2j+1}} \frac{\beta_{j'j}}{K_\beta}[d^\dagger_\pi \times \tilde{a}_{j'}]^{(j)}_m \\ & - \sum_{j'} \frac{v_j}{\sqrt{N_\pi}} \sqrt{\frac{10}{2j+1}} \frac{\beta_{j'j}}{K_\beta}[(s^\dagger_\pi \times \tilde{d}_\pi)^{(2)} \times a^\dagger_{j'}]^{(j)}_m.\end{aligned} \tag{23}$$

Another possibility is to use the version of the transfer operator deduced using the generalized Holstein-Primakoff

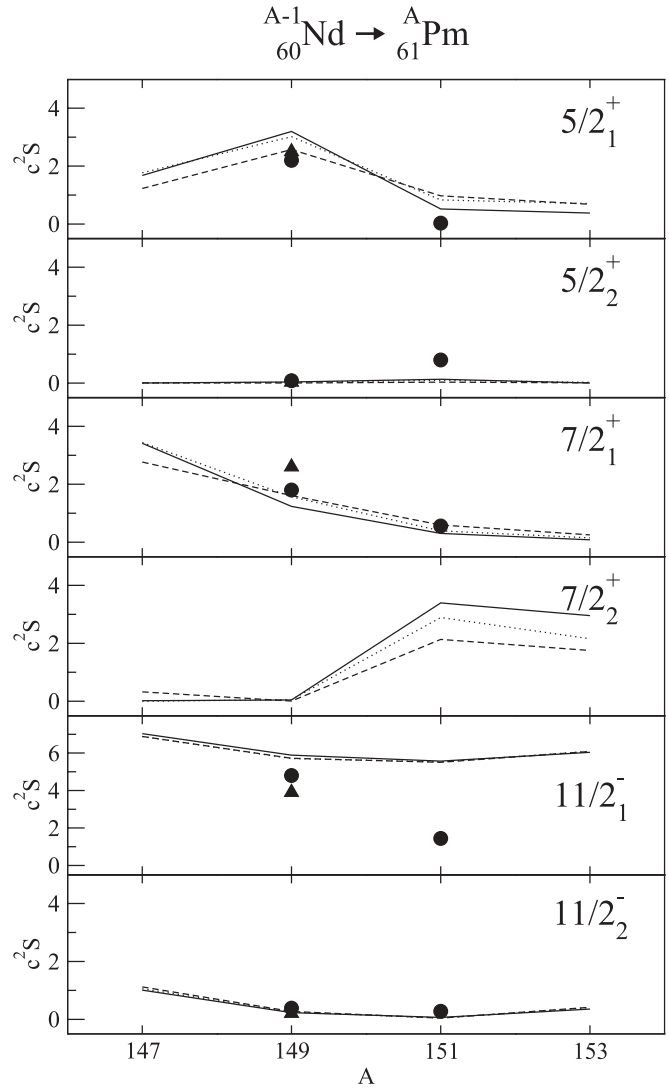

FIG. 12. Experimental [16–19] and calculated spectroscopic factors corresponding to one-proton stripping reactions. Circles and triangles indicate data obtained from (^{3}He, d) and (α, t) reactions, respectively. Solid, dotted, and dashed lines correspond to results obtained with the FO, GS, and HP transfer operators, respectively.

(HP) scheme [23], suitable for deformed nuclei. The form of this operator is [24]

$$\begin{aligned}(\hat{T}_{jm})_{\rm HP} = {} & u_j a^\dagger_{jm} + \sum_{j'\lambda} (-1)^{\lambda+j'-j} X^\lambda_{j'j} \frac{\hat{\lambda}}{\hat{j}} (\gamma^\dagger_\lambda \times \tilde{a}_{j'})^{(j)}_m \\ & - \sum_{\substack{j'j''L_1L_2\lambda \\ L_1=L_2\neq 0}} \frac{(-1)^{j'+j''+L_2}}{2u_{j'}} X^{L_1}_{jj''} X^{L_2}_{j'j''} \\ & \times \frac{\hat{\lambda}\hat{L}_1\hat{L}_2}{\hat{j}} \begin{Bmatrix} j & j' & \lambda \\ L_2 & L_1 & j'' \end{Bmatrix} [(\gamma^\dagger_{L_1} \times \tilde{\gamma}_{L_2})^{(\lambda)} \times a^\dagger_{j'}]^{(j)}_m,\end{aligned} \tag{24}$$

where $\hat{\lambda} = \sqrt{2\lambda+1}$, $\gamma^\dagger_\lambda$ refers to $s^\dagger_\pi$ ($\lambda = 0$) and $d^\dagger_\pi$ ($\lambda = 2$), and the quantities $X^\lambda_{jj'}$ are given by the expressions

$$X^0_{jj} = \frac{\hat{j} v_j}{\sqrt{N_\pi}}, \tag{25}$$

$$X^2_{jj'} = \frac{\sqrt{2}(v_j + v_{j'})\langle j||Y^2||j'\rangle}{\sqrt{\sum_{jj'}[(v_j + v_{j'})\langle j||Y^2||j'\rangle]^2}}. \tag{26}$$

Stripping reactions from ^{A}Nd to $^{A+1}$Pm are characterized by preserving the number of bosons, in the language of the IBFM-2. In the above expressions, only the terms which conserve the number of bosons contribute to the spectroscopic factors for these reactions. In order to calculate them, we will use three different approximations for the transfer operator: (i) the FO operator which is the common term in both the GS and HP transfer operators, (ii) the GS operator, which contains the FO operator with the addition of terms of the type $[(s^\dagger_\pi \times \tilde{d}_\pi)^{(2)} \times a^\dagger_{j'}]^{(j)}_m$ for different values of j', and (iii) the HP operator, which, in addition to the terms in the GS operator, includes terms of the type $[(d^\dagger_\pi \times \tilde{s}_\pi)^{(2)} \times a^\dagger_{j'}]^{(j)}_m$ and $[(d^\dagger_\pi \times \tilde{d}_\pi)^{(\lambda)} \times a^\dagger_{j'}]^{(j)}_m$ for different values of j' and λ. Terms of the type $[(d^\dagger_\pi \times \tilde{s}_\pi)^{(2)} \times a^\dagger_{j'}]^{(j)}_m$ are forbidden in the GS operator at the approximation usually used, since they change seniority in three units, while the terms $[(d^\dagger_\pi \times \tilde{d}_\pi)^{(\lambda)} \times a^\dagger_{j'}]^{(j)}_m$ can be present in the GS, but they belong to a higher order correction in the boson expansion.

Figure 12 shows the spectroscopic factors obtained with the three transfer operators, normalized according to the McFarlane sum rules, along with the experimental values from two different reactions [16–19]. The calculated values with the three approximations used for the transfer operator are very similar. This means that the corrections to the FO operator are small. The calculations reproduce the behavior of the experimental values except for the transfer to the $11/2^-_1$ level in ^{151}Pm. Additional experimental information would be crucial in order to elucidate which is the best choice for the transfer operator, especially for the transfer to the $7/2^+_2$ levels in ^{151}Pm and ^{153}Pm for which the different operators yield appreciably different results.

The targets in the one-proton pickup reactions leading to ^{A}Pm are the $^{A+1}$Sm isotopes. The wave functions for these isotopes were obtained using the same Hamiltonian as the one used for the Nd isotopes, with parameters taken from Ref. [10], quoted in Table VII.

TABLE VII. Parameters different from zero (ϵ and κ in MeV) used to calculate the wave functions of the Sm isotopes ($N_\pi = 6$). The values $\xi = 0.12$, $\chi_\pi = -1.3$, and $C^{(\pi)}_2 = 0.05$ MeV are the same for all the isotopes.

A	148	150	152	154
N_ν	2	3	4	5
ϵ	0.95	0.70	0.52	0.43
κ	−0.12	−0.08	−0.075	−0.081
χ_ν	0.00	−0.80	−1.00	−1.10

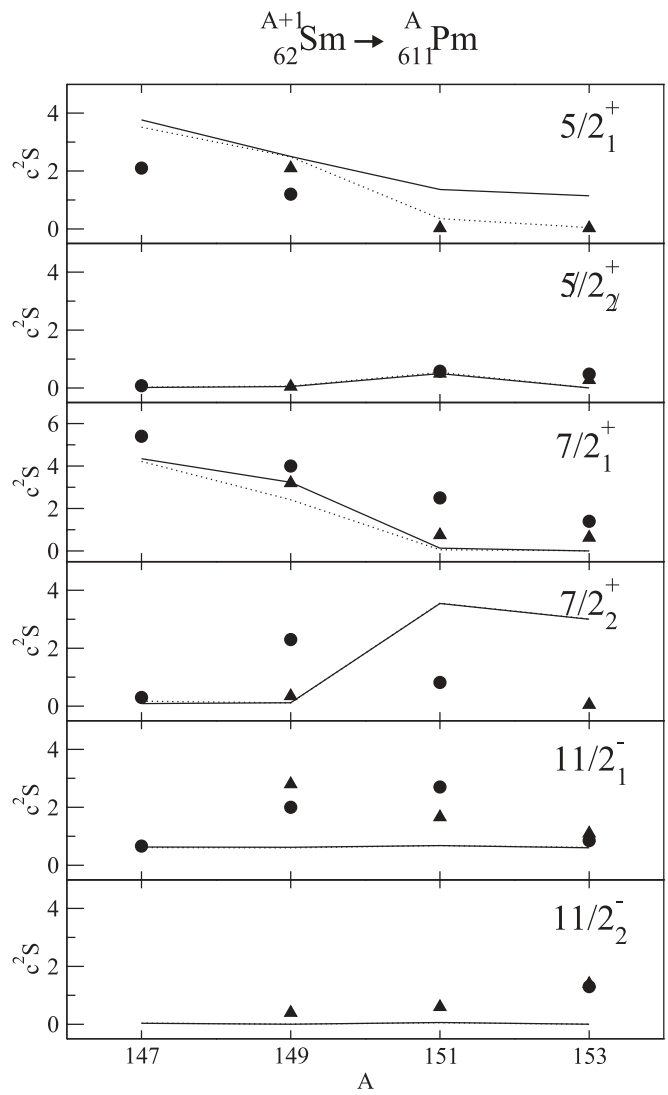

FIG. 13. Experimental [16–19,25] and calculated spectroscopic factors corresponding to one-proton pickup reactions. Circles and triangles indicate data obtained from (d,^{3}He) and (t, α), respectively. Solid and dotted lines correspond to the results obtained with the GS and HP transfer operators, respectively.

In this case, the number of bosons is not preserved and only terms of the type $(\gamma^\dagger_\lambda \times \tilde{a}_{j'})^{(j)}_m$ contribute to the spectroscopic factors. Two calculations have been performed, corresponding to the GS and HP transfer operators, respectively. Calculated spectroscopic factors have been normalized to reproduce the spectroscopic sum rules. Figure 13 shows the results of the calculations along with the experimental data [16–19,25]. In contrast to the stripping reactions, there is more experimental data available for the pickup ones, which allows a more detailed comparison with the calculated values. Both calculations are rather similar and reproduce qualitatively the experimental data, with the exception of those of the $7/2^+_2$ levels. The largest differences between the GS and the HP calculations can be found in the $5/2^+_1$ levels for the more deformed isotopes. In this area the HP operator reproduces

better the experimental data, according to the scheme in which it has been deduced, suitable for deformed nuclei.

IV. CONCLUSIONS

In the present work we have performed a comprehensive theoretical description of odd-even Pm isotopes from $A = 147$ to 153 in terms of the IBFM-2. Positive and negative parity states have been studied in an independent way, taking into account the main single-particle degrees of freedom involved in each case.

From the wave functions obtained in such study we get different observables, such as $E2$ and $M1$ transition probabilities and moments, and spectroscopic factors for one-proton transfers, involving a Pm isotope. For the latter we have used several possibilities for the transfer operator, in order to establish under which conditions each one is more appropriate.

We conclude that the general trend of the observables studied is well accounted for in this study, reproducing the transitional behavior observed in the experimental data. The strength of the different terms of the boson-fermion interaction have been kept constant along the isotopic chain. Fine tuning of the parameters would be needed in order to get a better description for each particular nucleus.

As far as the one-particle transfer is concerned, more experimental data in the studied region would be desirable in order to be able to make strong statements on the appropriateness of each of the different transfer operators existing in the literature.

In closing, we would like to point out that, in several places in this paper, discrepancies between the calculations and experimental data have been attributed to couplings of the fermions with boson states that are outside the used boson space (like 3^-_1, or an excited 0^+ that cannot be reproduced without including the octupole degree of freedom). It should be clear that we have restrictions in our own fermion model space that could be in part the origin of the discrepancies. We have restricted the fermion space to $d_{5/2}$, $g_{7/2}$, and $h_{11/2}$ orbitals. One could think that by including $d_{3/2}$, $s_{1/2}$, and $f_{7/2}$, some of the discrepancies could be corrected. The effective parameters in a larger space would, of course, be different. Small contributions, of the order of a few percent (10% to 15%), of $d_{3/2}$ or $s_{1/2}$ for positive parity states ($f_{7/2}$ for negative parity states) in the wave functions could in principle have sizable effects on the calculations. However, preliminary calculations in this enlarged fermion space have not confirmed a significant improvement in the agreement with the experimental data. Therefore, we think that the boson space limitation is mainly responsible for the discrepancies found, but a thorough study could be in order.

ACKNOWLEDGMENTS

This work has been supported by the Spanish Ministerio de Ciencia e Innovación under Projects No. FIS2009-07277 and No. FIS2008-04189, by CPAN-Ingenio (CSPD-2007-00042-Ingenio 2010), and by Junta de Andalucía (FQM160, P07-FQM-02962). J.B. is funded by CSIC under a JAE postdoctoral contract.

[1] G. G. Adamian, N. V. Antonenko, R. V. Jolos, and T. M. Schneidman, Phys. Rev. C **70**, 064318 (2004).
[2] F. Iachello and A. Arima, *The Interacting Boson Model* (Cambridge University, Cambridge, UK, 1987).
[3] F. Iachello and P. V. Isacker, *The Interacting Boson-Fermion Model* (Cambridge University, Cambridge, UK, 1991).
[4] A. Arima and F. Iachello, Phys. Rev. Lett. **35**, 1069 (1975).
[5] O. Scholten and T. Ozzello, Nucl. Phys. A **424**, 221 (1984).
[6] G. Audi, A. Wapstra, and C. Thibault, Nucl. Phys. A **729**, 337 (2003).
[7] N. Stone, At. Data Nucl. Data Tables **90**, 75 (2005).
[8] C. Alonso, J. Arias, and M. Lozano, J. Phys. G **14**, 877 (1988).
[9] J. Barea, Ph.D. thesis, University of Seville, 2002.
[10] O. Scholten, Ph.D. thesis, University of Groningen, 1980.
[11] J. Margraf *et al.*, Phys. Rev. C **47**, 1474 (1993).
[12] B. Reehal and R. Sorensen, Phys. Rev. C **2**, 819 (1970).
[13] O. Scholten and N. Blasi, Nucl. Phys. A **380**, 509 (1982).
[14] D. Bucurescu, G. Cata-Danil, N. V. Zamfir, A. Gizon, and J. Gizon, Phys. Rev. C **43**, 2610 (1991).
[15] G. Cata-Danil, D. Bucurescu, A. Gizon, and J. Gizon, J. Phys. G **20**, 1051 (1994).
[16] N. Nica, Nucl. Data Sheets **110**, 749 (2009).
[17] B. Singh, Nucl. Data Sheets **102**, 1 (2004).
[18] B. Singh, Nucl. Data Sheets **110**, 1 (2009).
[19] R. G. Helmer, Nucl. Data Sheets **107**, 507 (2006).
[20] M. Sambataro, O. Scholten, A. Dieperink, and G. Piccitto, Nucl. Phys. A **423**, 333 (1984).
[21] V. E. Iacob, W. Urban, J. C. Bacelar, J. Jongman, J. Nyberg, G. Sletten, and L. Trache, Nucl. Phys. A **596**, 155 (1996).
[22] T. Otsuka, A. Arima, and F. Iachello, Nucl. Phys. A **309**, 1 (1978).
[23] C. Alonso, J. Arias, J. Dukelsky, and S. Pittel, Nucl. Phys. A **539**, 391 (1992).
[24] J. Dukelsky and S. Pittel, in *Perspectives for the Interacting Boson Model on the Occasion of Its 20th Anniversary*, edited by R. F. Casten, A. Vitturi, A. B. Balantekin, B. R. Barrett, J. N. Ginocchio, G. Maino, and T. Otsuka (World Scientific, Singapore, 1994), p. 291.
[25] I. S. Lee, W. J. Jordan, J. V. Maher, R. Kamermans, J. W. Smits, and R. H. Siemssen, Nucl. Phys. A **371**, 111 (1981).